Observation of Time-Domain Rabi Oscillations in the Landau-Zener Regime with a Single Electronic Spin

Jingwei Zhou,[1,2] Pu Huang,[1,2] Qi Zhang,[1,2] Zixiang Wang,[1,2] Tian Tan,[1,2] Xiangkun Xu,[1,2] Fazhan Shi,[1,2] Xing Rong,[1,2] S. Ashhab,[3,4] and Jiangfeng Du[1,2,*]

[1]*Hefei National Laboratory for Physics Sciences at Microscale and Department of Modern Physics, University of Science and Technology of China, Hefei, Anhui 230026, China*

[2]*Synergetic Innovation Center of Quantum Information and Quantum Physics, University of Science and Technology of China, Hefei, Anhui 230026, China*

[3]*Advanced Science Institute, RIKEN, Wako-shi, Saitama 351-0198, Japan*

[4]*Qatar Environment and Energy Research Institute, Doha, Qatar*

(Received 21 April 2013; revised manuscript received 22 August 2013; published 9 January 2014)

It is theoretically known that the quantum interference of a long sequence of Landau-Zener transitions can result in Rabi oscillations. Because of its stringent requirements, however, this phenomenon has never been experimentally observed in the time domain. Using a nitrogen-vacancy (NV) center spin in isotopically purified diamond, we observed the Rabi oscillations resulting from more than 100 Landau-Zener processes. Our results demonstrate favorable quantum controllability of NV centers, which could find applications in quantum metrology and quantum information processing.

DOI: 10.1103/PhysRevLett.112.010503 PACS numbers: 03.67.Lx, 42.50.Dv, 76.60.-k, 76.70.Hb

The phenomenon of Rabi oscillations (ROs), first studied in 1937 [1], occurs in almost any quantum system under the influence of resonant external driving and is at the heart of various spectroscopic techniques. Landau-Zener (LZ) transitions, first studied in 1932 [2–5], are also ubiquitous in quantum systems, typically occurring when two energy levels of a quantum system undergo an avoided crossing.

It is known that interference between multiple LZ transitions can produce periodic Rabi oscillations (LZROs) [6,7]. One of the main requirements for the observation of such LZROs is that the coherence time of the quantum system must be long enough to allow the coherent interference between a long sequence of LZ processes.

With the recent advances in various quantum systems [8,9], a number of experiments have been able to demonstrate the controlled interference of LZ transitions. Interference between two LZ transitions has been observed in gaseous molecules [10], semiconductor-based quantum dots [11], NV centers [12], and atoms in optical lattices [13]. Evidence for various interference effects involving multiple LZ transitions has been observed in the steady-state behavior of continuously driven superconducting qubits [14,15] and nitrogen-vacancy (NV) centers [16]. However, Rabi oscillations in the LZ regime have never been observed experimentally because of the limited coherence times in those systems.

In this Letter, we report the experimental observation of LZROs resulting from the interference between more than 100 LZ processes. LZROs exhibit a number of phenomena that are qualitatively different from ROs in the weak-driving regime, such as different behaviors in the fast- and slow-passage regimes, as well as completely destructive interference between consecutive LZ transitions. Furthermore, our experimental results show that the decay of the LZROs with frequency modulation is suppressed relative to that of ROs in the usual case of resonant-fixed-frequency-driving Rabi oscillations (RFFROs) under the same driving microwave (MW) power. Experimental results indicate that the dominant contribution to the decay of LZROs comes from the fluctuation of the MW amplitude, and this conclusion is supported by theoretical calculations. The observed LZROs with suppressed decay may provide potential applications in quantum control and broaden the scope of studying a variety of quantum dynamical phenomena using NV centers.

A NV center consists of a substitutional N atom with an adjacent vacant site (V) in the diamond crystal lattice. It has an electron spin-1 ground state with three sublevels, $|m_s = 0\rangle$ and $|m_s = \pm 1\rangle$, quantized along the [111] crystal axis [Fig. 1(a)]. Quantum logic gates [17,18], quantum entanglement generation [19], single-shot readout [20–22], quantum memory operations [23], and quantum algorithms [24,25] have been realized in such systems. These achievements make NV centers in diamond a promising candidate as a platform for building quantum computers. Furthermore, with their favorable coherence properties and atomic-scale size, NV centers have also been used for sensing magnetic fields with nanometer spatial resolution [26,27].

The sample used in our experiment is an isotopically pure ^{12}C (> 99.9%) diamond with NV centers being created at about 5–10 nm below the surface by ^{15}N ion implantation of 5 keV in energy [28]. When an externally applied magnetic field is aligned with the principal axis of the NV center, the Hamiltonian for the NV center is

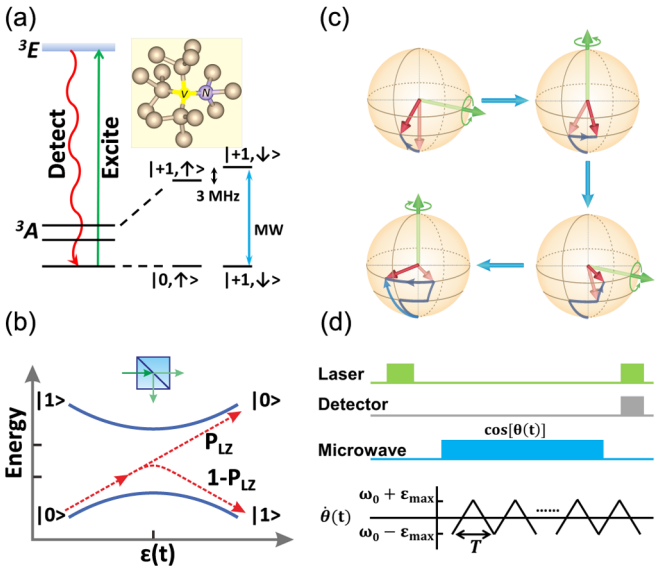

FIG. 1 (color online). (a) Schematic diagram of a NV center in the diamond lattice and the energy level diagram of the NV center. (b) Schematic diagram of Landau-Zener transition: when the energy levels undergo an avoided crossing, the quantum state undergoes a mixing process between the lower and the upper instantaneous eigenstates of the LZ Hamiltonian given by Eq. (2). This process is analogous to the operation of a beam splitter in optics experiments. (c) A single driving period contains four elementary rotations, which can be combined to produce a single effective rotation. On short time scales, one can see that each period involves four different rotations. On long time scales, the dynamics is described by the repeated application of the single-period rotation, as is the case for Rabi oscillations. (d) The pulse sequence used to drive Rabi oscillations in the LZ regime.

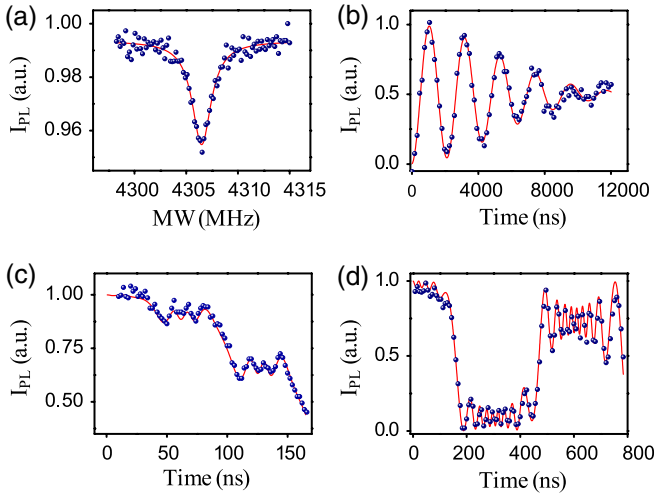

FIG. 2 (color online). (a) Photoluminescence (PL) intensity of the optically detected magnetic resonance spectrum for the transition between the states $|0\rangle$ and $|1\rangle$ of the NV center (blue dots). The red curve is a fit with a single Lorentzian peak. (b) Results of a standard Ramsey experiment on the NV center. The results are fitted to the function $\exp[-(t/T_2^*)^2]\cos(2\pi\delta_f t)$ ($\delta_f = 0.56$ MHz), where the oscillations are due to the detuning between the MW signal and the $|0\rangle \leftrightarrow |1\rangle$ transition. (c),(d) The occupation probability of the state $|0\rangle$ for a double-passage experiment in the fast- and slow-passage regimes.

$$H = DS_z^2 + \gamma_e B S_z + A_{zz} I_z S_z. \tag{1}$$

Here, $D = 2.87\,\mathrm{GHz}$, $\gamma_e = 2.8\,\mathrm{MHz/G}$, and $A_{zz} = -3.05\,\mathrm{MHz}$ are the parameters for the zero-field splitting, the Zeeman interaction, and the hyperfine interaction between the electron spin and the ^{15}N nuclear spin ($I = 1/2$) of the NV center, respectively. By applying a static magnetic field of 510 G, the degeneracy of the states $|m_s = \pm 1\rangle$ is lifted, and the nitrogen nuclear spin is polarized to be $I_z = -1/2$ by optical pumping [29] throughout the experiment. In our experiments we use the states $|m_s = 0\rangle$ and $|m_s = +1\rangle$ for the qubit's states $|0\rangle$ and $|1\rangle$, respectively. The optically detected magnetic resonance spectrum for the $|0\rangle \rightarrow |1\rangle$ transition is plotted in Fig. 2(a). The appearance of a single ESR peak confirms the polarization of the nearby nuclear spin. The free-induction-decay signal, shown in Fig. 2(b), gives a rather long dephasing time of $T_2^* = 6.6 \pm 0.2\ \mu$s, and spin-echo measurements (data not shown) give approximately $T_2 = 140\ \mu$s.

In order to induce transitions between the states $|0\rangle$ and $|1\rangle$, MW fields are generated using a local oscillator mixed with an arbitrary-waveform generator and then irradiated to the NV center via a coplanar waveguide [scheme in Fig. 1(d)]. The form of the variable-frequency MW signal is $2\Delta\cos[\theta(t)]$, with $\omega(t) = \dot{\theta}(t)$ being the instantaneous frequency, which deviates from the resonance frequency of the $|0\rangle \leftrightarrow |1\rangle$ transition by $\varepsilon(t) = \omega(t) - \omega_0 = \varepsilon_0 + \varepsilon_1(t)$ (ε_0 denoting its static offset part). After transforming the Hamiltonian to an appropriate rotating frame and adopting the rotating-wave approximation, the Hamiltonian for the qubit is simplified to the standard form:

$$H = \frac{\varepsilon(t)}{2}\sigma_z + \frac{\Delta}{2}\sigma_x. \tag{2}$$

We use a triangle wave for the function $\varepsilon(t)$:

$$\varepsilon(t) = \begin{cases} -\varepsilon_m + \frac{4\varepsilon_m(t-nT)}{T}, & t \in \left(n, n+\frac{1}{2}\right)T \\ \varepsilon_m - \frac{4\varepsilon_m(t-[n+1/2]T)}{T}, & t \in \left(n+\frac{1}{2}, n+1\right)T, \end{cases}$$

where $2\varepsilon_m$ and T are, respectively, the range and the period of the function $\varepsilon(t)$, and $n = 0, 1, 2, \ldots$. When the system is initialized in the state $|0\rangle$ and $\varepsilon(t)$ is swept through the value zero, a simple LZ transition occurs. The probability of the transition from $|0\rangle$ to $|1\rangle$ is given by the LZ formula [Fig. 1(b)]:

$$P_{|0\rangle\rightarrow|1\rangle} = 1 - P_{\mathrm{LZ}} = 1 - \exp\left(-\frac{\pi}{2}\frac{\Delta^2}{v}\right), \tag{3}$$

where v is the sweep rate of the diabatic energy difference at the crossing. For the triangle wave used in our experiment, $v = 4\varepsilon_m/T$.

For a slow sweep, the system transforms adiabatically from $|0\rangle$ to $|1\rangle$. As the sweep rate increases, P_{LZ} decreases following the exponential-decay function given in Eq. (3). The value of Δ can be obtained in this way, which is always found to agree with the values obtained using resonant driving [30]. In Figs. 2(c) and 2(d), we show the results for double-passage Landau-Zener-Stückelberg (LZS) interferometry in the fast- and slow-passage regimes corresponding to P_{LZ} close to 1 and 0, respectively. The short-time dynamics clearly shows steplike LZ transitions with small-amplitude, high-frequency oscillations, and this is in good agreement with numerical simulations. The oscillations are a result of the fact that even far away from the avoided crossing point the σ_x term in the Hamiltonian still induces some dynamics in the populations of the two basis states [31].

We now consider the effects of strong, periodic driving of the NV center. LZS interference can be understood using an analogy with Mach-Zehnder interferometry in an optical setup [14]. This analogy provides a good understanding of the LZS setup when dealing with one or two LZ processes. For analyzing the resonance phenomena associated with continuous driving of the system, a geometric picture is more intuitive [7,15]. When the two-level quantum system is driven through the avoided crossing region, the lower and upper states are mixed together in a process that can be described by the following matrix [30]:

$$N = \begin{pmatrix} \alpha & -\gamma^* \\ \gamma & \alpha^* \end{pmatrix}, \tag{4}$$

where $\alpha = \sqrt{1 - P_{\mathrm{LZ}}}e^{-i\varphi}$ and $\gamma = \sqrt{P_{\mathrm{LZ}}}$, with φ being a geometric phase associated with the LZ transition [6]. In the geometric picture, the LZ mixing processes is represented by a rotation about an axis that depends on the various parameters described above. Between LZ processes the system is moved away from the avoided crossing and brought back some time later, such that a phase accumulates between the two quantum states. This phase is given by the integral over time of the energy separation between the two energy levels $2\zeta = \int (E_e - E_g)dt$, and the corresponding quantum process U is represented by a rotation about the z axis.

A full driving cycle is therefore composed of four rotations alternating between two different axes [Fig. 1(c)]. This sequence of four rotations is equivalent to a single rotation ($G_1 = U_2 N U_1 N$); depending on the various angles involved, the axis for the net rotation can point in any direction. Specifically, the matrix G_1 describing the net rotation has the same form as Eq. (4), but with parameters α and γ that can be lengthy in general [6].

By stringing a large number of these rotations together, we obtain a resonance effect. If the axis of the single-period net rotation points in the xy plane, the resonance condition is satisfied. Even if the mixing between the lower and upper states in a single driving period is small, the rotations of multiple periods will add up constructively, and we obtain full oscillations between the states $|0\rangle$ and $|1\rangle$. If the axis of the single-period net rotation points outside the xy plane, there can be partial, but not full, conversion between the two states.

Two opposite limits are of particular interest: fast (almost sudden, $1 - P_{\mathrm{LZ}} \ll 1$) and slow (almost adiabatic, $P_{\mathrm{LZ}} \ll 1$) passage. In both cases, we observe steplike dynamics that reflect LZ processes associated with the passage through the avoided crossing, as well as RO dynamics at long time scales. To observe ROs in different regimes, we first vary the sweep rate. In Fig. 3(a), we set $\varepsilon_m/\Delta = 18.0$ (well in the LZ regime) and $v = 2\pi \times 3.12$ MHz/ns, which gives $P_{\mathrm{LZ}} = 0.91$ (fast-passage regime). We observe coherent oscillations that result from the quantum interference of a sequence containing over 100 LZ processes. These oscillations are observed up to about 8 μs without any appreciable steady decay. In Fig. 3(b), we set $\varepsilon_m/\Delta = 5.25$ (LZ regime) and $v = 2\pi \times 0.33$ MHz/ns, which gives $P_{\mathrm{LZ}} = 0.064$ (slow-passage regime). The measured and calculated curves clearly

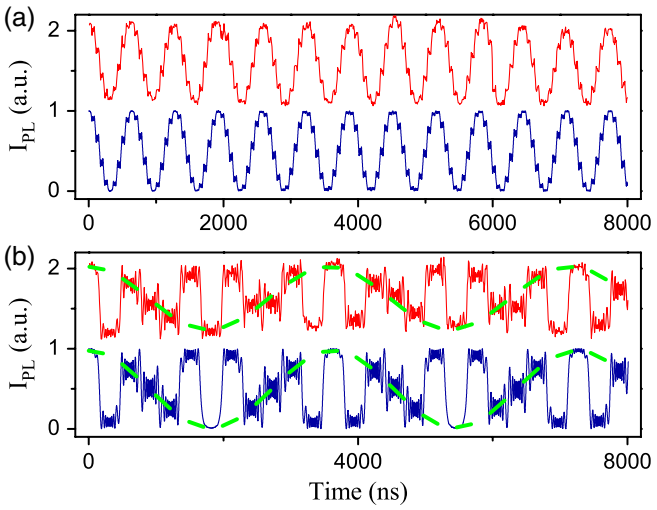

FIG. 3 (color online). Rabi oscillations resulting from the interference of many LZ processes. (a) Fast-passage regime. The measured (upper curve) and numerically simulated (lower line) occupation probabilities P_0 of the state $|0\rangle$ as a function of time. The experimental data here and those in (b) are offset along the y axis for visibility. The Rabi frequency is about 1.49 MHz, which is consistent with numerical simulations. The parameters used in this case are $\Delta = 2\pi \times 5.57$ MHz, $\varepsilon_m = 2\pi \times 100$ MHz, and $T = 128$ ns. (b) Slow-passage regime. The same as in (a), except that dashed sinusoidal envelopes are added to show the oscillatory behavior, which corresponds to the ROs in the adiabatic basis. The parameters used in this case are $\Delta = 2\pi \times 9.60$ MHz, $\varepsilon_m = 2\pi \times 50.4$ MHz, and $T = 606$ ns.

show many steps associated with LZ processes at short time scales, as well as long-time oscillatory envelopes. The RO pattern is more clearly recognizable when transformed to the adiabatic basis $[|e(\epsilon)\rangle, |g(\epsilon)\rangle]$. The results in the adiabatic basis are well fitted with a sinusoidal function in Fig. 3(b). The ROs in the slow-passage regime are in some sense more impressive than those in the fast-passage regime. Every passage through the avoided crossing is now almost adiabatic, such that the quantum state changes drastically in the natural basis $(|0\rangle, |1\rangle)$ every time the system goes through the avoided crossing [30]. Nevertheless, quantum coherence is preserved, and the interference of over 15 LZ processes is observed without any discernible decay.

Rabi oscillations are also obtained in the case of intermediate sweep rates and intermediate degrees of constructive (or destructive) interference between successive LZ processes [30]. The effect of varying the degree of constructive interference is illustrated in Fig. 4. Taking the parameters of Fig. 3(a) and changing T from 128 to 149 ns, the constructive interference between successive LZ processes is replaced by completely destructive interference. This situation corresponds to the so-called coherent destruction of tunneling [32], where the $|0\rangle \rightarrow |1\rangle$ transition is suppressed not because the driving is nonresonant, but because the parameters are chosen such that the single-period net rotation gives the identity operation (i.e., it has a zero rotation angle).

We now analyze the decay of the observed oscillations. We measured the LZROs shown in Fig. 3(a) for an extended period of 80 μs [30], from which we obtain the decay time $T'_{2,\mathrm{LZRO}} = 58 \pm 3$ μs. The noise contributing to the decay of

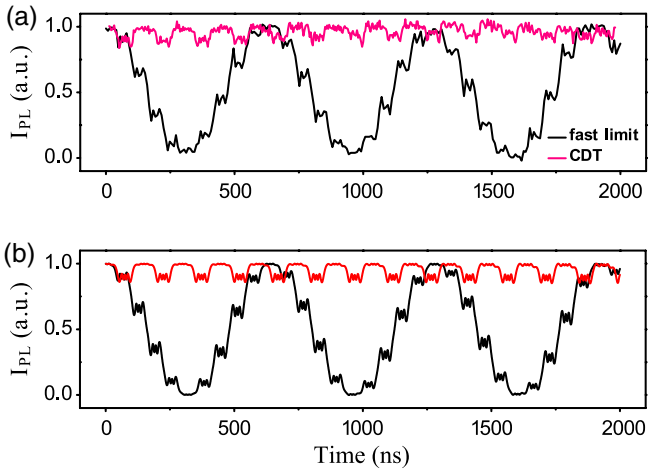

FIG. 4 (color online). Constructive versus destructive interferences in a single driving period. The parameters are the same as in Fig. 3(a), except for the sweep period being $T = 149$ ns in the case of destructive interference (pink line). The experimental results are shown in (a), while the results of numerical simulations are shown in (b). The case of destructive interference corresponds to the phenomenon of coherent destruction of tunneling (CDT).

LZROs (and also RFFROs) can be attributed to two main sources: fluctuations in the driving field and sources that are intrinsic to the sample, such as the noise due to the nuclear spin bath, various paramagnetic centers in the diamond sample, and other surface-related contributions [33] for a near-surface NV center. Detailed experimental studies together with theoretical analysis [30] considering both types of noise indicate that the dominant contribution to the decay of the LZROs (and RFFROs) in our experiment is due to the fluctuation of the driving field amplitude.

In a previous study [12], we were only able to observe a limited number of LZ transitions. In this study, using an isotopically purer sample, the long coherence time allows the observation of many more LZ transitions, so that LZROs can be clearly demonstrated. T'_{LZRO} is a few times longer than $T'_{\mathrm{RFFRO}} = 17 \pm 1$ μs measured for RFFROs under the same MW power, showing the suppression of the decay in LZROs relative to RFFROs.

When the fluctuation of the MW field amplitude is the dominant noise source and the intrinsic noise is neglected, theoretical calculations [30] relate the LZRO and RFFRO decay times by the following expression

$$\frac{T'_{2,\mathrm{LZRO}}}{T'_{2,\mathrm{RFFRO}}} = \frac{1}{|J_n(x)|}, \tag{5}$$

where J_n is the Bessel function and n denotes n-photon resonance. For a sinusoidal function $\varepsilon(t) = \varepsilon_0 + A\cos(\omega t)$, $n = \varepsilon_0/\omega$ and $x = A/\omega$. For the symmetric triangle wave used in our experiments, $n = 0$ and $x \approx 4\varepsilon_m T/\pi^3$. It should be noted that since $|J_n(x)| < 1$, at least for the case where the intrinsic noise is negligible, $T'_{2,\mathrm{LZRO}}$ is always longer than $T'_{2,\mathrm{RFFRO}}$ and can be greatly extended for the case of small $|J_n(x)| < 1$. The enhancement factor predicted for the current experiment using Eq. (5) is 4.08, comparable with the measured value of 3.41. The agreement is good considering the approximations of keeping only the dominant contribution that leads to Eq. (5).

In summary, using a single electron spin in diamond, we have observed Rabi oscillations resulting from the quantum interference of more than 100 LZ processes in various regimes ranging from slow to fast passage and from constructive to destructive interference within a single driving period. The experimental observation of the quantum oscillations in the LZ regime verifies the rich dynamics of a fundamental paradigm, which may be explored for the study of some fundamental phenomena, such as magnetic resonance beyond the rotating-wave approximation [34] and multiphoton transitions [14]. For the isotopically purified diamond used in our experiment, the decay time for LZROs is longer than that for ROs with fixed-frequency driving under the same driving power. Taking advantage of such multiple passages and favorable coherence properties of NV centers, LZROs might also be exploited for potential applications in quantum metrology and quantum

information processing, such as the measurement of geometric phases [35,36] and quantum gates based on LZS interference [37,38].

We thank J. Wrachtrup from the University of Stuttgart for providing the isotopically purified diamond sample, Yiqun Wang from the Suzhou Institute of Nano-Tech and Nano-Bionics for fabricating the coplanar waveguide, and Changkui Duan for helpful discussions. This work was supported by the National Key Basic Research Program of China (Grant No. 2013CB921800), the National Natural Science Foundation of China (Grants No. 11227901, No. 11275183, No. 11274299, No. 91021005, and No. 10834005), the 'Strategic Priority Research Program (B)' of the CAS (Grant No. XDB01030400), and the Fundamental Research Funds for the Central Universities.

*djf@ustc.edu.cn

[1] I. I. Rabi, Phys. Rev. **51**, 652 (1937).
[2] L. Landau, Phys. Z. Sowjetunion **1**, 88 (1932); L. Landau, Phys. Z. Sowjetunion **2**, 46 (1932).
[3] C. Zener, Proc. R. Soc. A **137**, 696 (1932).
[4] E. C. G. Stueckelberg, Helv. Phys. Acta **5**, 369 (1932).
[5] E. Majorana, Nuovo Cimento **9**, 43 (1932).
[6] S. N. Shevchenko, S. Ashhab, and F. Nori, Phys. Rep. **492**, 1 (2010).
[7] S. Ashhab, J. R. Johansson, A. M. Zagoskin, and F. Nori, Phys. Rev. A **75**, 063414 (2007).
[8] T. D. Ladd, F. Jelezko, R. Laflamme, Y. Nakamura, C. Monroe, and J. L. O'Brien, Nature (London) **464**, 45 (2010).
[9] I. Buluta, S. Ashhab, and F. Nori, Rep. Prog. Phys. **74**, 104401 (2011).
[10] M. Mark, T. Kraemer, P. Waldburger, J. Herbig, C. Chin, H.-C. Nägerl, and R. Grimm, Phys. Rev. Lett. **99**, 113201 (2007).
[11] J. R. Petta, H. Lu, and A. C. Gossard, Science **327**, 669 (2010).
[12] P. Huang, J. Zhou, F. Fang, X. Kong, X. Xu, C. Ju, and J. Du, Phys. Rev. X **1**, 011003 (2011).
[13] S. Kling, T. Salger, C. Grossert, and M. Weitz, Phys. Rev. Lett. **105**, 215301 (2010).
[14] W. D. Oliver, Y. Yu, J. C. Lee, K. K. Berggren, L. S. Levitov, and T. P. Orlando, Science **310**, 1653 (2005).
[15] M. Sillanpää, T. Lehtinen, A. Paila, Yu. Makhlin, and P. Hakonen, Phys. Rev. Lett. **96**, 187002 (2006).
[16] L. Childress and J. McIntyre, Phys. Rev. A **82**, 033839 (2010).
[17] F. Jelezko, T. Gaebel, I. Popa, A. Gruber, and J. Wrachtrup, Phys. Rev. Lett. **92**, 076401 (2004).
[18] F. Jelezko, T. Gaebel, I. Popa, M. Domhan, A. Gruber, and J. Wrachtrup, Phys. Rev. Lett. **93**, 130501 (2004).
[19] P. Neumann, N. Mizuochi, F. Rempp, P. Hemmer, H. Watanabe, S. Yamasaki, V. Jacques, T. Gaebel, F. Jelezko, and J. Wrachtrup, Science **320**, 1326 (2008).
[20] B. B. Buckley, G. D. Fuchs, L. C. Bassett, and D. D. Awschalom, Science **330**, 1212 (2010).
[21] P. Neumann, J. Beck, M. Steiner, F. Rempp, H. Fedder, P. R. Hemmer, J. Wrachtrup, and F. Jelezko, Science **329**, 542 (2010).
[22] L. Robledo, L. Childress, H. Bernien, B. Hensen, Paul F. A. Alkemade, and R. Hanson, Nature (London) **477**, 574 (2011).
[23] G. D. Fuchs, G. Burkard, P. V. Klimov, and D. D. Awschalom, Nat. Phys. **7**, 789 (2011).
[24] F. Shi, X. Rong, N. Xu, Y. Wang, J. Wu, B. Chong, X. Peng, J. Kniepert, R. S. Schoenfeld, W. Harneit, M. Feng, and J. Du, Phys. Rev. Lett. **105**, 040504 (2010).
[25] T. van der Sar, Z. H. Wang, M. S. Blok, H. Bernien, T. H. Taminiau, D. M. Toyli, D. A. Lidar, D. D. Awschalom, R. Hanson, and V. V. Dobrovitski, Nature (London) **484**, 82 (2012).
[26] G. Balasubramanian, I. Y. Chan, R. Kolesov, M. AlHmoud, J. Tisler, C. Shin, C. Kim, A. Wojcik, Philip R. Hemmer, A. Krueger, T. Hanke, A. Leitenstorfer, R. Bratschitsch, F. Jelezko, and J. Wrachtrup, Nature (London) **455**, 648 (2008).
[27] J. R. Maze, P. L. Stanwix, J. S. Hodges, S. Hong, J. M. Taylor, P. Cappellaro, L. Jiang, M. V. Gurudev Dutt, E. Togan, A. S. Zibrov, A. Yacoby, R. L. Walsworth, and M. D. Lukin, Nature (London) **455**, 644 (2008).
[28] S. Pezzagna, B. Naydenov, F. Jelezko, J. Wrachtrup, and J. Meijer, New J. Phys. **12**, 065017 (2010).
[29] V. Jacques, P. Neumann, J. Beck, M. Markham, D. Twitchen, J. Meijer, F. Kaiser, G. Balasubramanian, F. Jelezko, and J. Wrachtrup, Phys. Rev. Lett. **102**, 057403 (2009).
[30] See Supplemental Material at http://link.aps.org/supplemental/10.1103/PhysRevLett.112.010503 for the materials and method, analytical theory, and decoherence on the Rabi oscillations in Landau-Zener regime.
[31] D. M. Berns, M. S. Rudner, S. O. Valenzuela, K. K. Berggren, W. D. Oliver, L. S. Levitov, and T. P. Orlando, Nature (London) **455**, 51 (2008).
[32] F. Grossmann, T. Dittrich, P. Jung, and P. Hänggi, Phys. Rev. Lett. **67**, 516 (1991).
[33] A. Laraoui, J. S. Hodges, and C. A. Meriles, Nano Lett. **12**, 3477 (2012).
[34] G. D. Fuchs, V. V. Dobrovitski, D. M. Toyli, F. J. Heremans, and D. D. Awschalom, Science **326**, 1520 (2009).
[35] X. Rong, P. Huang, X. Kong, X. Xu, F. Shi, Y. Wang, and J. Du, Europhys. Lett. **95** 60 005 (2011).
[36] J. Zhang, J. Zhang, X. Zhang, and K. Kim, arXiv:1304.0271.
[37] H. Ribeiro, G. Burkard, J. R. Petta, H. Lu, and A. C. Gossard, Phys. Rev. Lett. **110**, 086804 (2013).
[38] G. Cao, H. Li, T. Tu, L. Wang, C. Zhou, M. Xiao, C. Guo, H. Jiang, and G. Guo, Nat. Commun. **4**, 1401 (2013).